Quantitative assessment of the impact of climate change on creep of concrete structures

Nasr, Amro; Kjellström, Erik; Larsson Ivanov, Oskar; Johansson, Jonas; Björnsson, Ivar; Honfi, Daniel

Published in:
Proceedings of the 31st European Safety and Reliability Conference (ESREL 2021)

DOI:
10.3850/978-981-18-2016-8_539-cd

2021

Document Version:
Publisher's PDF, also known as Version of record

Quantitative assessment of the impact of climate change on creep of concrete structures

Amro Nasr

Division of Structural Engineering, Lund University, Sweden. E-mail: amro.nasr@kstr.lth.se
Department of Public Works Engineering, Faculty of Engineering, Mansoura University, Egypt

Erik Kjellström

Rossby Centre, Swedish Meteorological and Hydrological Institute, Sweden. E-mail: erik.kjellstrom@smhi.se

Oskar Larsson Ivanov

Division of Structural Engineering, Lund University, Sweden. E-mail: oskar.larsson_ivanov@kstr.lth.se
Boverket, National Board of Housing, Building and Planning, Sweden.

Jonas Johansson

Division of Risk Management and Societal Safety, Lund University, Sweden. E-mail: jonas.johansson@risk.lth.se

Ivar Björnsson

Division of Structural Engineering, Lund University, Sweden. E-mail: ivar.bjornsson@kstr.lth.se

Dániel Honfi

Monitoring and Analyses of Existing Structures, Ramboll, Denmark. E-mail: dhon@ramboll.com

Creep of concrete structures is in most cases regarded as a serviceability problem that may have impacts on maintenance and repair costs but cannot lead to structural collapse. However, several structural collapses during the past decades have been, at least partly, attributed to excessive creep deformations. Recent studies suggest that concrete creep may be further exacerbated by climate change. The current study demonstrates how this effect can be quantitatively assessed. For this purpose, six different creep models (i.e, Model Code 1999, Model Code 2010, MPF, B3, B4, and B4s models) are used under considerations of historical and future climatic conditions in southernmost Sweden as given by a regional climate model. Furthermore, two different simulations were performed as follows: 1) considering only climate uncertainty represented by the climate model, and 2) considering climate uncertainty, parameter uncertainty, and creep model uncertainty. The highest impact of climate change on end of century creep coefficient is observed using model B4 where the 75th percentile of the increase in creep coefficient is found to range from ~8% to ~14% depending on the climate scenario. The results of the assessment in this article show that the uncertainty related to climate change on creep of concrete structures (higher effect in RCP8.5 than in RCP2.6 and RCP4.5 which have very similar results) is much smaller than uncertainties resulting from creep modelling.

Keywords: Climate change, Long-term deformations, Creep, Creep models, Creep coefficient, Parameter uncertainty, Model uncertainty, Infrastructure safety, Infrastructure performance.

1. Introduction

Many potential climate change impacts on built infrastructure have been identified in recent studies (e.g., Nasr et al., 2019). According to the fifth assessment report (AR5) of the Intergovernmental Panel on Climate Change (IPCC), these impacts can significantly affect the performance and safety of many infrastructure elements (IPCC, 2014, Chapter 8). Several of these impacts have been assessed in a quantitative manner by the research community, such as accelerated deterioration of infrastructure (Bastidas-Arteaga and Stewart, 2015; Stewart et al., 2011) and increased scouring under submerged foundations of infrastructure (Dikanski et al., 2018). Nonetheless, many other identified potential impacts of climate change on built infrastructure have not yet been investigated quantitatively. One of these impacts is the potential increase in creep of concrete structures due to climate change, see Nasr et al. (2019).

Although creep of concrete structures mainly is a serviceability problem, it can lead to severe consequences. For instance, the collapse of the Koror–Babeldaob Bridge in Palau in 1996 can be, at least partly, attributed to excessive creep deformations (Bažant et al., 2011). In Bažant et al. (2011), 56 other bridges were found to show similar problems with creep deformations and many more probably exist. The progressive collapse of Roissy Charles de Gaulle Airport is another example where excessive creep

Proceedings of the 31st European Safety and Reliability Conference
Edited by Bruno Castanier, Marko Cepin, David Bigaud, and Christophe Berenguer
Published by Research Publishing, Singapore.
ISBN: 978-981-18-2016-8; doi:10.3850/978-981-18-2016-8_539-cd

deformation have contributed to more severe consequences affecting structural safety (El Kamari et al., 2015).

Many models for assessing creep of concrete structures exist. Examples of these models are: Model Code 1999 model (MC99) (Eurocode model) (CEN, 2004; FIB, 1999), Model code 2010 model (MC10) (FIB, 2010), ACI model (ACI, 1992), GL 2000 model (Gardner and Lockman, 2001), MPF model (Chateauneuf et al., 2014), B3 model (Bažant and Baweja, 2000), B4 model (Bažant et al., 2015), and B4s model (Bažant et al., 2015). It has been noted earlier that some of the models commonly used in practice, e.g., MC99 model and ACI model, tend to grossly underestimate multi-decade creep, see e.g., Bažant et al. (2012). This highlights the large model uncertainty that characterizes creep modelling.

Under this premise the aim of the current article is twofold. Firstly, a probabilistic approach for quantifying the impact of climate change on the creep of concrete structures is described and demonstrated. Secondly, the validity of the often-unchallenged assumption that climate change uncertainty dominates the other sources of uncertainty, e.g., parameter uncertainty and impact model uncertainty, involved in assessing the impacts of climate change on built infrastructure is investigated. The article starts by describing four different creep models in detail as well as their stochastic application and the climate model data used. The following section presents an illustrative example that demonstrates the applicability of creep models in assessing the impact of climate change on creep. Lastly, the final section highlights some concluding remarks.

2. Creep Modelling

As previously mentioned, there exists many models for predicting the creep of concrete structures. In this section, four such models are described in detail; MC99, B3, B4, and B4s. Although models MC10 and MPF are also used in the next section, they are not described in this section for the sake of brevity. Depending on the model used, creep of a concrete structure at age t due to a compressive stress σ applied at age t' is described by either the creep coefficient $\varphi(t,t')$ or the creep compliance $J(t,t')$. The relationship between $\varphi(t,t')$ and $J(t,t')$ is described by the following expression (e.g., Bažant et al., 2015):

$$\varepsilon_\sigma(t) = J(t,t')\sigma = \left(\frac{\varphi(t,t')+1}{E(t')}\right)\sigma \quad (1)$$

Where $\varepsilon_\sigma(t)$ is the stress-dependent strain (i.e., excluding shrinkage and thermal strains) at age t and $E(t')$ is the modulus of elasticity at loading age t'.

2.1. *MC99 model (Eurocode model)*

The MC99 model (FIB, 1999) predicts $\varphi(t,t')$ as follows:

$$\varphi(t,t') = \varphi_0\beta_c(t,t') \quad (2)$$

with

$$\varphi_0 = \varphi_{RH,T}\beta(f_{cm})\beta(t') \quad (3)$$

$$\varphi_{RH,T} = \varphi_T + (\varphi_{RH}-1){\varphi_T}^{1.2} \quad (4)$$

$$\varphi_T = e^{0.015(T-20)} \quad (5)$$

$$\varphi_{RH} = \left(1+\frac{1-\frac{RH}{100}}{0.1\sqrt[3]{h}}\alpha_1\right)\alpha_2 \quad (6)$$

$$\alpha_1 = \left(\frac{35}{f_{cm}}\right)^{0.7}, \alpha_2 = \left(\frac{35}{f_{cm}}\right)^{0.2} \quad (7)$$

$$\beta(f_{cm}) = \frac{16.8}{\sqrt{f_{cm}}} \quad (8)$$

$$\beta(t') = \frac{1}{0.1+(t'_{adj})^{0.2}} \quad (9)$$

$$t'_{adj} = t'\left(\frac{9}{2+(t')^{1.2}}+1\right)^{\alpha} \geq 0.5\ days \quad (10)$$

$$\alpha = \begin{Bmatrix} -1 & class\ 32.5N\ (class\ S) \\ 0 & classes\ 32.5R, 42.5N\ (class\ N) \\ 1 & classes\ 42.5R, 52.5N, 52.5R\ (class\ R) \end{Bmatrix} \quad (11)$$

$$\beta_c(t,t') = \left(\frac{t-t'}{\beta_{H,T}+(t-t')}\right)^{0.3} \quad (12)$$

$$\beta_{H,T} = \beta_H\beta_T \quad (13)$$

$$\beta_H = 1.5h(1+(0.012RH)^{18}) + 250\alpha_3 \leq 1500\alpha_3 \quad (14)$$

$$\alpha_3 = \left(\frac{35}{f_{cm}}\right)^{0.5} \quad (15)$$

$$\beta_T = e^{\left(\frac{1500}{273+T}-5.12\right)} \quad (16)$$

where φ_0 is the notional creep coefficient, $\beta_c(t,t')$ is the creep time development function, T is the temperature in [^{o}C], RH is the relative humidity in [%], h is the notional size of the concrete member in [mm], f_{cm} is the mean compressive strength of concrete at the age of 28 days in [MPa], t and t' are the age and age at loading, respectively, in [days], t'_{adj} is the adjusted age at loading based on cement type and α is cement-type dependent factor.

The factors φ_T (Eq. (5)) and β_T (Eq. (16)) represent the effect of temperature on the creep coefficient and on the time development of creep, respectively. For a temperature of 20 ^{o}C (the default temperature of the model) both factors equal 1.0 and Eq. (4) and (13) reduce to the relative humidity dependent factors φ_{RH} and β_H, respectively. It is worth noting that, the adjustment of the age at loading according to the curing temperature is not considered here as this is not expected to be influenced by climate change. Furthermore, the transient creep coefficient that accounts for a sudden increase in temperature while the member is under load (e.g., due to fire) is not considered.

2.2. *B3 model*

The B3 model (Bažant and Baweja, 2000) predicts $J(t,t')$ (in [1/MPa]) as follows:

$$J(t,t') = \left(q_1 + C_0(t,t') + C_d(t,t',t_0)\right)\cdot 10^{-6} \quad (17)$$

with

$$C_0(t,t') = q_2Q(t,t') + q_3\ln(1+(t-t')^{0.1}) + q_4\ln\left(\frac{t}{t'}\right) \quad (18)$$

$$C_d(t,t',t_0) = \begin{Bmatrix} q_5\left(e^{-8H(t)} - e^{-8H(t'_0)}\right)^{0.5} & t \geq t'_0 \\ 0 & t < t'_0 \end{Bmatrix} \quad (19)$$

$$q_1 = \frac{600000}{E(28)} \quad (20)$$

$$E(28) = 4734\sqrt{f_{cm}} \quad (21)$$

$$q_2 = 185.4\, c^{0.5} {f_{cm}}^{-0.9} \quad (22)$$

$$q_3 = 0.29 \left(\frac{w}{c}\right)^4 q_2 \quad (23)$$

$$q_4 = 20.3 \left(\frac{a}{c}\right)^{-0.7} \quad (24)$$

$$Q(t,t') = Q_f(t')\left(1 + \left(\frac{Q_f(t')}{Z(t,t')}\right)^{r(t')}\right)^{-\frac{1}{r(t')}} \quad (25)$$

$$Q_f(t') = \left(0.086(t')^{\frac{2}{9}} + 1.21(t')^{\frac{4}{9}}\right)^{-1} \quad (26)$$

$$Z(t,t') = (t')^{-0.5} \ln(1 + (t-t')^{0.1}) \quad (27)$$

$$r(t') = 1.7(t')^{0.12} + 8 \quad (28)$$

$$q_5 = 7.57 \cdot 10^5 {f_{cm}}^{-1} |\varepsilon_{sh\infty} \cdot 10^6|^{-0.6} \quad (29)$$

$$\varepsilon_{sh\infty} = \varepsilon_{s\infty} \frac{E(607)}{E(t_0+\tau_{sh})} \quad (30)$$

$$\varepsilon_{s\infty} = -\alpha_1\alpha_2(0.019 w^{2.1} {f_{cm}}^{-0.28} + 270) \cdot 10^{-6} \quad (31)$$

$$\alpha_1 = \begin{Bmatrix} 1.0 & Type\ I\ cement \\ 0.85 & Type\ II\ cement \\ 1.1 & Type\ III\ cement \end{Bmatrix} \quad (32)$$

$$\alpha_2 = \begin{Bmatrix} 0.75 & Steam\ curing \\ 1.2 & Sealed \\ 1.0 & Curing\ in\ water \end{Bmatrix} \quad (33)$$

$$E(t) = E(28)\left(\frac{t}{4+0.85t}\right)^{0.5} \quad (34)$$

$$H(t) = 1 - (1 - RH_d)S(t) \quad (35)$$

$$S(t) = tanh\sqrt{\frac{t-t_0}{\tau_{sh}}} \quad (36)$$

$$\tau_{sh} = k_t (k_s h)^2 \quad (37)$$

$$k_t = 8.5 {t_0}^{-0.08} {f_{cm}}^{-0.25} \cdot 10^{-2} \quad (38)$$

$$k_s = \begin{Bmatrix} 1.00 & Infinite\ slab \\ 1.15 & Infinite\ cylinder \\ 1.25 & Infinite\ square\ prism \\ 1.30 & Sphere \\ 1.55 & Cube \end{Bmatrix} \quad (39)$$

$$t_0' = \max(t', t_0) \quad (40)$$

where q_1 is the instantaneous strain due to a unit stress, $C_0(t,t')$ is the compliance function for basic creep, $C_d(t,t',t_0)$ is the compliance function for drying creep, t_0 is the age when drying starts (i.e., age at exposure) in [days], q_2, q_3, q_4, and q_5 are empirical constitutive parameters, $E(28)$ is the modulus of elasticity at 28 days in [MPa], c, w, and a are the cement, water, and aggregate contents, respectively, in [kg/m^3], $\varepsilon_{sh\infty}$ is the ultimate shrinkage strain, $E(t)$ is the modulus of elasticity at age t, τ_{sh} is the shrinkage half-time in [days], RH_d is the relative humidity expressed as a decimal (e.g., 0.7 for 70% relative humidity), $S(t)$ is the shrinkage time function, and f_{cm}, h, t, and t' are as defined previously.

The effect of temperature on basic creep is accounted for by replacing Eq. (18) with Eq. (41) as follows:

$$C_0(t,t') = R_T\left(q_2 Q(t_T,t') + q_3 \ln(1 + (t_T - t')^{0.1}) + q_4 \ln\left(\frac{t_T}{t'}\right)\right) \quad (41)$$

with

$$R_T = e^{\frac{U_c'}{R}\left(\frac{1}{293} - \frac{1}{T_K}\right)} \quad (42)$$

$$t_T - t' = \beta_T'(t - t') \quad (43)$$

$$\beta_T' = e^{\frac{U_c}{R}\left(\frac{1}{293} - \frac{1}{T_K}\right)} \quad (44)$$

$$\frac{U_c}{R} = 3418\, w^{-0.27} {f_{cm}}^{0.54} \quad (45)$$

$$\frac{U_c'}{R} = 615.24\, w^{-0.27} {f_{cm}}^{0.54} \quad (46)$$

where t_T is the temperature adjusted age in [days], U_c' and U_c are the activation energies of creep describing the magnification and acceleration of creep due to a temperature increase, R is the gas constant, and T_K is the temperature in [Kelvin]. Although it is acknowledged that temperature also affects drying creep (see e.g., Bažant and Kim (1992)), this effect is not considered in the description of model B3. Similar to MC99, the adjustment of the age at loading according to the curing temperature is not considered.

2.3. *B4 and B4s models*

The B4 model (Bažant et al., 2015) predicts $J(t,t')$ (in [1/MPa]) as follows:

$$J(t,t') = q_{1,B4} + C_{0,B4}(t,t') + C_{d,B4}(t,t',t_0) \quad (47)$$

with

$$C_{0,B4}(t,t') = q_{2,B4} Q(t,t') + q_{3,B4} \ln(1 + (t-t')^{0.1}) + q_{4,B4} \ln\left(\frac{t}{t'}\right) \quad (48)$$

$$C_{d,B4}(t,t',t_0) = \begin{Bmatrix} q_{5,B4}\langle e^{-p_{5H}H(t)} - e^{-p_{5H}H(t_0')}\rangle^{0.5} & t \geq t_0' \\ 0 & t < t_0' \end{Bmatrix} \quad (49)$$

$$q_{1,B4} = \frac{p_1}{E(28)} \quad (50)$$

$$q_{2,B4} = p_2\left(\frac{w}{0.38c}\right)^{p_{2w}} \cdot 10^{-3} \quad (51)$$

$$q_{3,B4} = p_3 q_{2,B4}\left(\frac{a}{6c}\right)^{p_{3a}}\left(\frac{w}{0.38c}\right)^{p_{3w}} \quad (52)$$

$$q_{4,B4} = p_4\left(\frac{a}{6c}\right)^{p_{4a}}\left(\frac{w}{0.38c}\right)^{p_{4w}} \cdot 10^{-3} \quad (53)$$

$E(28)$, $Q(t,t')$, $Q_f(t')$, $Z(t,t')$, and $r(t')$ as in model B3, see Eq. (21), and (25)-(28), respectively.

$$q_{5,B4} = p_5\left(\frac{a}{6c}\right)^{p_{5a}}\left(\frac{w}{0.38c}\right)^{p_{5w}} \left|k_h \varepsilon_{sh\infty,B4}(t_0)\right|^{p_{5\varepsilon}} \cdot 10^{-3} \quad (54)$$

$$k_h = \begin{Bmatrix} 1 - {RH_d}^3 & RH_d \leq 0.98 \\ 12.94(1 - RH_d) - 0.2 & 0.98 < RH_d \leq 1 \end{Bmatrix} \quad (55)$$

$$\varepsilon_{sh\infty,B4}(t_0) = -\varepsilon_0 k_{\varepsilon a} \frac{E(607)}{E(t_0+\tau_{sh,B4})} \quad (56)$$

$$\varepsilon_0 = \varepsilon_{cem}\left(\frac{a}{6c}\right)^{p_{\varepsilon a}}\left(\frac{w}{0.38c}\right)^{p_{\varepsilon w}}\left(\frac{6.5c}{\rho}\right)^{p_{\varepsilon c}} \quad (57)$$

$$\tau_{sh,B4} = \tau_0 k_{\tau a}(k_s h)^2 \quad (58)$$

$$\tau_0 = \tau_{cem}\left(\frac{a}{6c}\right)^{p_{\tau a}}\left(\frac{w}{0.38c}\right)^{p_{\tau w}}\left(\frac{6.5c}{\rho}\right)^{p_{\tau c}} \quad (59)$$

$E(t)$, $H(t)$, $S(t)$, and k_s, as in model B3, see Eq. (34)-(36) and (39), respectively.

where p_{5H}, p_1, p_2, p_3, p_4, p_5, p_{2w}, p_{3a}, p_{3w}, p_{4a}, p_{4w}, p_{5a}, p_{5w}, $p_{5\varepsilon}$, ε_{cem}, $p_{\varepsilon a}$, $p_{\varepsilon w}$, $p_{\varepsilon c}$, τ_{cem}, $p_{\tau a}$, $p_{\tau w}$, and $p_{\tau c}$ are cement-type dependent parameters (see Bažant et al. (2015)) ,$\langle u \rangle = \max(u, 0)$, k_h is a humidity-dependent factor, $k_{\varepsilon a}$ and $k_{\tau a}$ are aggregate-type dependent parameters (see Bažant et al. (2015)), ρ is the density of

concrete (taken as 2350 kg/m^3), and all the other parameters are as defined previously with the subscript B4 indicating model B4.

Model B4s is a simplified version of model B4 which depends only on f_{cm}. In this model, the same Equations of model B4 are used except that Eq. (51)-(54), (57), and (59), respectively, are replaced as follows:

$$q_{2,B4s} = s_2 \left(\frac{f_{cm}}{40}\right)^{s_{2f}} \cdot 10^{-3} \quad (60)$$

$$q_{3,B4s} = s_3 q_{2,B4s} \left(\frac{f_{cm}}{40}\right)^{s_{3f}} \quad (61)$$

$$q_{4,B4s} = s_4 \left(\frac{f_{cm}}{40}\right)^{s_{4f}} \cdot 10^{-3} \quad (62)$$

$$q_{5,B4s} = s_5 \left(\frac{f_{cm}}{40}\right)^{s_{5f}} \cdot \left|k_h \varepsilon_{sh\infty,B4s}(t_0)\right|^{p_{5\varepsilon}} 10^{-3} \quad (63)$$

$$\varepsilon_{0,B4s} = \varepsilon_{s,cem} \left(\frac{f_{cm}}{40}\right)^{s_{\varepsilon f}} \quad (64)$$

$$\tau_{0,B4s} = \tau_{s,cem} \left(\frac{f_{cm}}{40}\right)^{s_{\tau f}} \quad (65)$$

where s_2, s_3, s_4, s_5, s_{2f}, s_{3f}, s_{4f}, s_{5f}, $\varepsilon_{s,cem}$, $\tau_{s,cem}$, $s_{\varepsilon f}$, and $s_{\tau f}$ are cement-type dependent parameters (see Bažant et al. (2015)), $\varepsilon_{sh\infty,B4s}$ is evaluated as in Eq. (56) but with replacing ε_0 by $\varepsilon_{0,B4s}$, and f_{cm} and $p_{5\varepsilon}$ are as defined previously.

The effect of temperature in B4 and B4s models is considered in the same way as in model B3 (see Eq. (41)-(46)) but with two main differences. The first difference is that $\frac{U_c}{R}$ and $\frac{U_c'}{R}$ are assumed to be equal and have a value of 4000 K (unless data for the given concrete is available and better values can be estimated). The second difference is that the temperature adjusted age t_T is used in evaluating both $C_0(t,t')$ and $C_d(t,t',t_0)$ instead of only $C_0(t,t')$ in model B3. The temperature adjustments of the age at loading and age at exposure are not considered in the context of this article as they are not expected to be influenced by climate change.

2.4. *Stochastic modelling of creep*

This subsection describes the stochastic application of the presented creep models. For modelling the parameter uncertainty, the uncertainty factors shown in Table 1 are multiplied by the respective parameter in each model. For modelling the creep model uncertainty in MC99 and B3 models, the uncertainty factors shown in Table 2 are multiplied by their corresponding equations in the same table. Lastly, for modelling the creep model uncertainty in models B4 and B4s, the uncertainty factors shown in Table 3 are multiplied by their corresponding equations in the same table.

Table 1. Parameter uncertainty factors; N: Normal distribution, LN: Lognormal distribution; COV: Coefficient of variation; The mean value for all factors is 1.0.

Factor	COV	Reference(s)
$\delta_{f_{cm}}$ (N)	0.15	Bažant and Baweja (2000)
δ_c (LN)	0.1	Bažant et al. (2015) for distribution type, Madsen and Bažant (1983) for COV
$\delta_{\frac{w}{c}}$ (LN)	0.1	e.g., Hamidane et al. (2020)
$\delta_{\frac{a}{c}}$ (LN)	0.1	e.g., Hamidane et al. (2020)
δ_h (N)	0.1019	Tu et al. (2017)

Table 2. Modelling uncertainty factors for models MC99 and B3; N: Normal distribution; COV: Coefficient of variation; The mean value for all factors is 1.0; The Equation(s) column shows the equations where these factors are multiplied.

Factor	COV	Reference(s)	Equation(s)
δ_{MC99} (N)	0.47	Wendner et al. (2015)	(2)
$\delta_{B3,1}$ (N)	0.366	Bažant and Baweja (2000) for distribution type, Wendner et al. (2015) for COV	(20), (22)-(24), and (29)
$\delta_{B3,2}$ (N)	0.422		(30)
$\delta_{B3,3}$ (N)	0.281	Bažant and Baweja (2000)	(42)

Table 3. Modelling uncertainty factors for models B4 and B4s; LN~(μ_{lnx}, σ_{lnx}): Lognormal distribution with the distribution parameters μ_{lnx} and σ_{lnx}; COV: Coefficient of variation; The Equation(s) column shows the equations where these factors are multiplied.

Factor	Distribution	Reference(s)	Equation (s)
$\delta_{B4,1}$	LN~(0.01,0.35)	Wendner et al. (2015)	(50)
$\delta_{B4,2}$	LN~(0.09,0.67)		(51)-(52) and (60)-(61)
$\delta_{B4,3}$	LN~(0.07,0.56)		(53) and (62)
$\delta_{B4,4}$	LN~(0.07,0.66)		(54) and (63)
$\delta_{B4,5}$	LN~(0.06,0.5)	Hubler et al. (2015)	(58)
$\delta_{B4,6}$	LN~(0.16,0.58)		(56)

2.5. *Climate model projections used in the study*

The climate data input to the creep modelling is taken from the RCA4 regional climate model (Kjellström et al., 2016) operated over Europe at 50x50 km grid spacing. We use aggregated data over the southernmost county in Sweden, Skåne, c. 11.000 km^2 for annual mean temperature and relative humidity. The climate change projections involve RCA4 downscaling nine global climate models (GCMs) under three scenarios of future radiative forcing, the so-called Representative Concentration Pathway scenarios RCP2.6, RCP4.5, and RCP8.5 (Moss et al., 2010). The

GCMs are: EC-EARTH, MIROC5, HadGEM2-ES, MPI-ESM-LR, and NorESM1-M for all three scenarios. In addition, CanESM2, IPSL-CM5A-MR, GFDL-ESM2M and CSIRO-Mk3-6-0 have been downscaled for RCP4.5 and RCP8.5. All GCMs have been used in the context of CMIP5 (the fifth phase of the coupled model intercomparison project), see Taylor et al. (2012). For a more comprehensive description of the RCA4 climate projections see Kjellström et al. (2016).

3. Illustrative Example

3.1. *Description*

For demonstrating the applicability of the described models in assessing the impact of climate change on concrete creep, the example presented in Bažant et al. (2015) based on test data from Nasser and Al-Manaseer (1986) is considered.

The following properties are given: 1) ASTM type I cement (corresponds to Class N, see Bažant et al. (2015)); 2) $t' = 28$ days; 3) $t_0 = 28$ days; 4) $f_{cm} = 27.6$ MPa; 5) $h = 38.1$ mm; 6) $c = 219.3$ kg/m^3; 7) $\frac{w}{c} = 0.6$; 8) $\frac{a}{c} = 7.0$; 9) $\sigma = 11.03$ MPa. It is assumed that the structure is an infinite slab built in 2020 in the southern county Skåne in Sweden, the curing is done in water, and the aggregate type is unknown. The slab is exposed to evolving climate conditions over 81 years until the end of 2100 when the creep coefficient is evaluated. Relative humidity and temperature data for these 81 years according to the different RCP scenarios (see, Figure 1) were used to assess the creep coefficient at 2100. Furthermore, the creep coefficient at 2100 was also assessed based on the historical (i.e., 1961-1990) climate data (see, Figure 1).

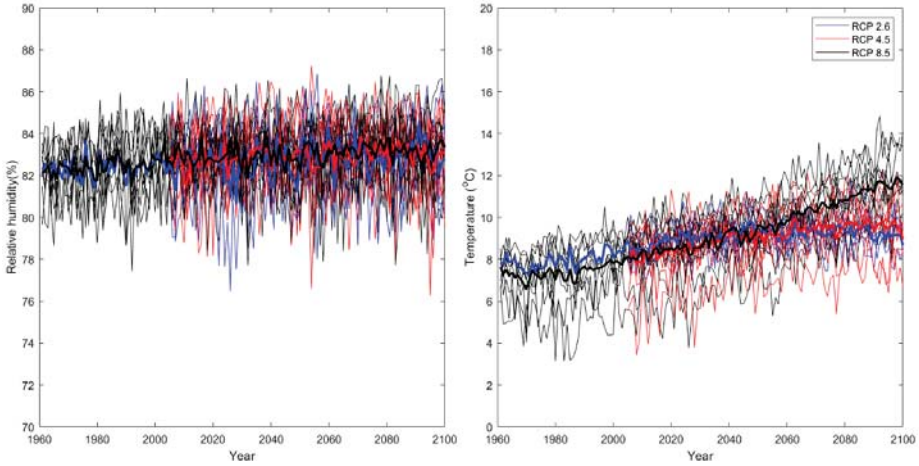

Fig. 1. Annual mean relative humidity and temperature as projected by RCA4 for Skåne, Sweden; multiple lines for each scenario represent different climate projections (five different climate projections for RCP2.6 and nine different climate projections for RCP4.5 and RCP8.5) and the bold lines represent the average of all climate models for each scenario.

3.2. *Results and discussion*

For assessing the impact of climate change on creep, two Monte Carlo simulations were performed as follows: 1) considering only climate uncertainty (based on the different climate projections shown in Figure 1), and 2) considering climate uncertainty, parameter uncertainty, and model uncertainty. In both simulations, the temperature and relative humidity data in each year were fitted to normal distributions and the results of MPF, B3, B4, and B4s models were converted to $\varphi(t, t')$ using the relationship in Eq. (1) for reasons of comparability.

Figure 1 shows that there is large interannual variability in both relative humidity and temperature according to the climate model. For relative humidity there is virtually no trend in the projections for future climate while for temperature a continued warming is seen in particular in the strongest scenario RCP8.5. RCP4.5 and RCP2.6 are seemingly relatively similar in their temperature evolution but it should be noted that the number of global climate models differ. RCP2.6 with stabilizing forcing towards the end of the century shows the weakest increase in temperature.

Figures 2 and 3 show the probability distributions of the resulting end of century creep coefficients using the different creep models under the different climatic conditions (i.e., historical, RCP2.6, RCP4.5, and RCP8.5) in the first and second simulations, respectively. Figure 2 shows that, when the other sources of uncertainty (i.e., parameter uncertainty and creep model uncertainty) are disregarded, climate change can have an observable impact on concrete creep. The results of models B4 and B4s show the highest percentile increase in end of century creep coefficient compared to the historical climate, while the results of model MPF show the lowest percentile increase (see Table 4). It can also be noted that model MPF gives the highest creep coefficient while model B3 gives the lowest

estimate of the creep coefficient. On the other hand, when parameter and creep model uncertainties are included in the simulation (see Figure 3), the different probability distributions of end of century creep coefficients overlap and the effect of climate change becomes harder to observe. This indicates that parameter and creep model uncertainties dominate over climate uncertainty.

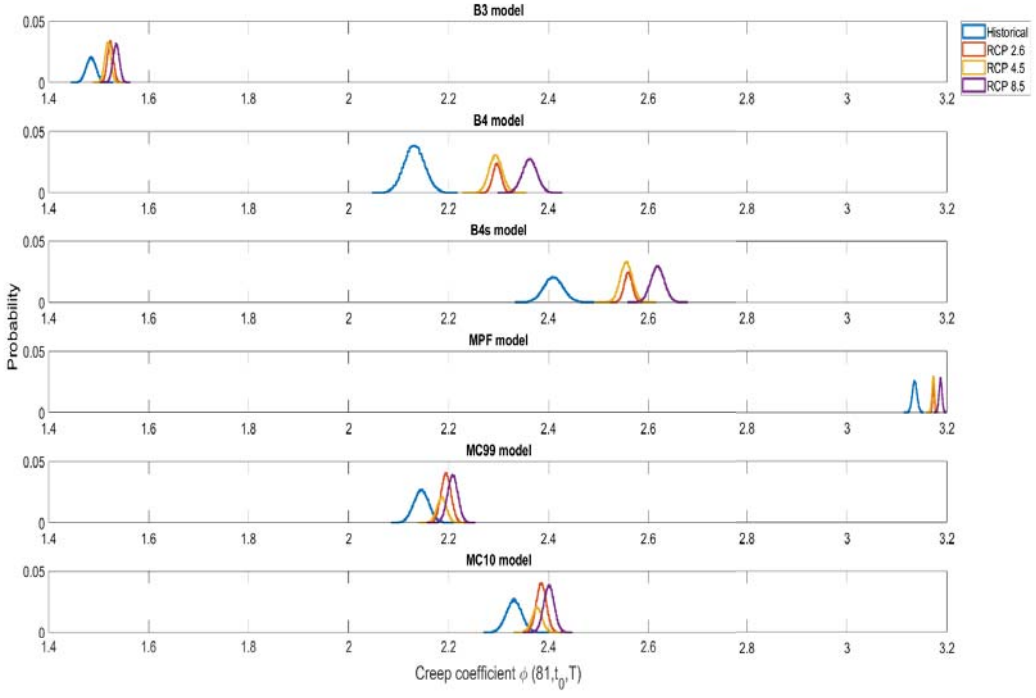

Fig. 2. Probability distributions of the end of century creep coefficients using the different creep models under the different climatic conditions (historic climate, RCP2.6, RCP4.5, and RCP8.5) considering only climate uncertainty.

Table 4. 25th and 75th percentile of the increase in end of century creep coefficient compared to the historical climate under different climate change scenarios using different creep models in the first and second simulations; highest and lowest values in each row are boldfaced and italicized, respectively.

Scenario	Simulation	Percentile	B3	B4	B4s	MPF	MC99	MC10
RCP2.6	1	25th	2.1%	**7.0%**	5.6%	*1.1%*	1.7%	1.8%
		75th	3.1%	**8.5%**	6.8%	*1.3%*	2.9%	2.9%
	2	25th	1.5%	**5.9%**	4.6%	*1.1%*	1.7%	1.8%
		75th	3.4%	**10.3%**	9.6%	*1.4%*	2.9%	2.9%
RCP4.5	1	25th	1.7%	**6.8%**	5.4%	*1.1%*	1.3%	1.4%
		75th	2.8%	**8.4%**	6.7%	*1.3%*	2.5%	2.5%
	2	25th	*1.1%*	**5.7%**	4.4%	*1.1%*	1.3%	1.4%
		75th	3.0%	**10.2%**	9.47%	*1.4%*	2.5%	2.5%
RCP8.5	1	25th	2.8%	**10.0%**	8.0%	*1.5%*	2.3%	2.5%
		75th	3.9%	**11.7%**	9.4%	*1.8%*	3.5%	3.6%
	2	25th	2.0%	**8.3%**	6.4%	*1.6%*	2.3%	2.4%
		75th	4.4%	**14.3%**	13.4%	*2.0%*	3.5%	3.5%

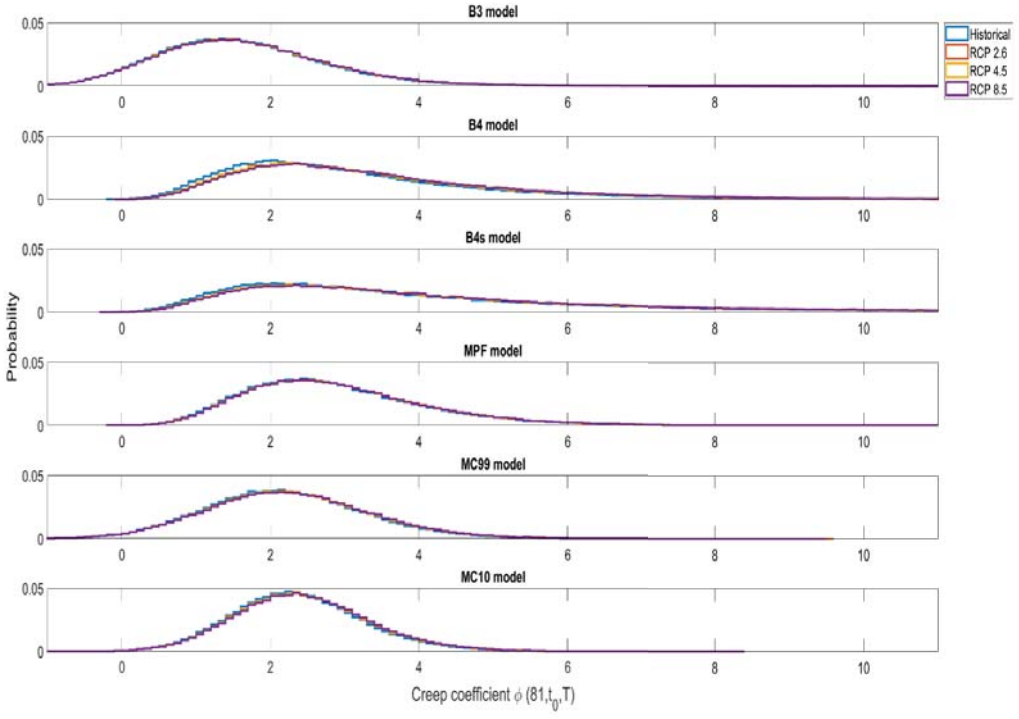

Fig. 3. Probability distributions of the end of century creep coefficients using the different creep models under the different climatic conditions (historic climate, RCP2.6, RCP4.5, and RCP8.5) considering climate, parameter, and creep model uncertainty.

The results in Table 4 further support this finding. Table 4 shows that, for all climate scenarios in both simulations, the highest percentile increase of end of century creep coefficient in comparison to the historical climate is found using model B4 while the lowest is found using model MPF. It is evident from this Table that the spread of the results across the different creep models for each scenario is significantly larger than across the different scenarios for each creep model. Table 4 also shows that the largest percentile increase in end of century creep coefficient is found for RCP8.5, while RCP2.6 and RCP4.5 give very similar results (with RCP2.6 slightly higher than RCP4.5). It should be noted, however, that RCP2.6 is not easily comparable to the other two scenarios due to the difference in the number of projections (five projections for RCP2.6 and nine projections for the other two scenarios). It is interesting to note, that the percentile increases in models MC99 and MC10 are very similar. Considering the previous results, it should be noted that in Wendner et al. (2015) model B4 was found to be the most accurate of all considered models excluding model MPF which was not considered in their study (followed by B4s, MC10, B3, and MC99, respectively).

4. Conclusions

Climate change can have potentially severe impacts on the safety and performance of infrastructure. One of these potential impacts is the increase of creep of concrete structures. Although creep is traditionally considered a serviceability issue, a number of structural collapses in the previous decades have been linked to excessive creep. This article describes and demonstrates how the effect of climate change on concrete creep can be assessed. For this purpose, six different creep models are used, namely: Model Code 1999, Model Code 2010, MPF, B3, B4, and B4s models. It is found that model B4 results in the highest percentile increase of end of century creep coefficient in comparison to the historical climate while model MPF results in the lowest percentile increase. Furthermore, the percentile increase is highest for RCP8.5 scenario with RCP2.6 and RCP4.5 resulting in very similar percentile increases. The increase is slightly higher in RCP2.6 than in RCP4.5 despite the fact that the forcing is smaller, we note, however, that the number of projections differ so that RCP2.6 is not easily comparable to the other two scenarios. An important finding

is that non-climate uncertainties (i.e., parameter and creep modelling uncertainties) dominate climate uncertainty in modelling the impact of climate change on creep of concrete structures. This is in contrast to the common belief that climate change uncertainty overshadows problems of climate change impact assessment.

Acknowledgements

The authors gratefully acknowledge the financial support provided by the Swedish Transport Administration, the Swedish Research Council (Formas), and the strategic innovation program InfraSweden2030, a joint effort of Sweden's Innovation Agency (Vinnova), the Swedish Research Council (Formas) and the Swedish Energy Agency (Energimyndigheten). Any opinions, findings, or conclusions stated herein are those of the authors and do not necessarily reflect the opinions of the financiers. Gustav Strandberg at SMHI is acknowledged for providing the climate model projections.

References

ACI Committee 209. (1992). Prediction of creep, shrinkage and temperature effects in concrete structures, ACI 209 R-92, American Concrete Institute, Detroit 1992.

Bastidas-Arteaga, E., and M. G. Stewart. (2015). Damage risks and economic assessment of climate adaptation strategies for design of new concrete structures subject to chloride-induced corrosion. Structural Safety, 52, 40–53.

Bažant, Z. P., and S. Baweja. (2000). Creep and shrinkage prediction model for analysis and design of concrete structures: Model B3. The Adam Neville symposium, A. Al-Manaseer, ed., ACI, Farmington Hills, MI, 1–83.

Bažant, Z. P., M. H. Hubler, and R. Wendner. (2015). RILEM draft recommendation: TC-242-MDC multi-decade creep and shrinkage of concrete: material model and structural analysis—Model B4 for creep, drying shrinkage and autogenous shrinkage of normal and high-strength concretes with multi-decade applicability. Materials and Structures, 48, 753–770.

Bažant, Z. P., M. H. Hubler, and Q. Yu. (2011). Pervasiveness of excessive segmental bridge deflections: Wake-up call for creep. ACI Structural Journal, 108(6), 766–774.

Bažant, Z. P., M. H. Hubler, and Q. Yu. (2015). Damage in prestressed concrete structures due to creep and shrinkage of concrete. Handbook of damage mechanics, Springer, New York.

Bažant, Z. P., and J.-K. Kim. (1992). Improved prediction model for time-dependent deformations of concrete: Part 4-Temperature effects. Materials and Structures, 25, 84–94.

Bažant, Z. P., Q. Yu., and G-H. Li. (2012). Excessive long-time deflections of prestressed box girders. II: Numerical analysis and lessons learned. J. Str. Eng., 138(6), 687–696.

CEN. (2004). Eurocode 2: Design of concrete structures -Part 1-1: General rules and rules for buildings, EN 1992-1-1. Part 2: Concrete bridges, EN 1992-1-2.

Chateauneuf, A, W. E. Raphael, and R. J. B. M. Pitti. (2014). Reliability of prestressed concrete structures considering creep models. Structure and Infrastructure Engineering, 10(12), 1595–1605.

Dikanski, H., B. Imam, and A. Hagen-Zanker. (2018). Effects of uncertain asset stock data on the assessment of climate change risks: A case study of bridge scour in the UK. Structural Safety, 71, 1–12.

El Kamari, Y., W. Raphael, and A. Chateauneuf. (2015). Reliability study and simulation of the progressive collapse of Roissy Charles de Gaulle Airport. Case Studies in Engineering Failure Analysis, 3, 88–95.

FIB. (1999). Structural concrete: textbook on behaviour, design and performance, updated knowledge of the CEB/FIP model Code 1990. Bulletin No. 2. Federation internationale du beton (FIB), Lausanne 1:35–52.

FIB. (2010). Model code 2010, Federation internationale du beton, Lausanne.

Gardner, N. J., and M. J. Lockman. (2001). Design provisions of shrinkage and creep of normal-strength concrete. ACI Mater. J, 98, 159–167.

Hamidane, H., A. Chateauneuf, A. Messabhia, and A. Ababneh. (2020). Reliability analysis of corrosion initiation in reinforced concrete structures subjected to chlorides in presence of epistemic uncertainties. Structural Safety, 86, 101976.

Hubler, M. H., R. Wendner, and Z. P. Bažant. (2015). Statistical justification of Model B4 for drying and autogenous shrinkage of concrete and comparisons to other models. Materials and Structures, 48, 797–814.

IPCC (Intergovernmental Panel on Climate Change). (2014). Climate Change 2014-Impacts, Adaptation, and Vulnerability-Part A: Global and Sectoral Aspects-Working Group II Contribution to the Fifth Assessment Report of the Intergovernmental Panel on Climate Change. Cambridge & New York: Cambridge University Press.

Kjellström, E., Bärring, L., Nikulin, G., Nilsson, C., Persson, G., and Strandberg, G., 2016. Production and use of regional climate model projections – a Swedish perspective on building climate services. Climate Services, 2-3, 15-29, DOI: 10.1016/j.cliser.2016.06.004.

Madsen, H. O., and Z. P. Bažant. (1983). Uncertainty analysis of creep and shrinkage effects in concrete structures. ACI Journal, 80, 116–127.

Moss, R.H., Edmonds, J.A., Hibbard, K.A., Manning, M.R., Rose, S.K., van Vuuren, D.P., 2010. The next generation of scenarios for climate change research and assessment. Nature 463. 10.1038/nature08823.

Nasr, A., I. Björnsson, O. Larsson Ivanov, J. Johansson, D. Honfi, and E. Kjellström. (2019). A review of the potential impacts of climate change on the safety and performance of bridges. Sus. Res. Inf. doi: 10.1080/23789689.2019.1593003

Nasser, K. W., and A. Al-Manaseer. (1986). Creep of concrete containing fly ash and superplasticizer at different stress/strength ratios. Am. Concr. Inst. J., 62, 668–673.

Raphael,W., F. Kaddah, F. Geara, J.-L. Favre, and J.-A. Calgaro. (2002). Nouveau modele de calcul pour la prediction du fluage du beton (in French). Annals of Buildings and Public Works, ITBTP,no. 5, France.

Stewart, M. G., X. Wang, and M. N. Nguyen. (2011). Climate change impact and risks of concrete infrastructure deterioration. Eng. Str., 33, 1326–1337.

Taylor, K.E., Stouffer, R.J., Meehl, G.A., 2012. An overview of CMIP5 and the experiment design. Bull. Am. Meteorol. Soc. 93, 485–498. http://dx.doi.org/10.1175/BAMS-D-11-00094.1.

Tu, B., Z. Fang, Y. Dong, and D. M. Frangopol. (2017). Time-variant reliability analysis of widened deteriorating prestressed concrete bridges considering shrinkage and creep. Eng. Str., 153, 1–16.

Wendner, R., M. H. Hubler, and Z. P. Bažant. (2015). Statistical justification of model B4 for multi-decade concrete creep using laboratory and bridge databases and comparisons to other models. Materials and Structures, 48, 815–833.